JACS
JOURNAL OF THE AMERICAN CHEMICAL SOCIETY
pubs.acs.org/JACS
Article

Photooxidation-Driven Purely Organic Room-Temperature Phosphorescent Lysosome-Targeted Imaging

Hua-Jiang Yu, Qingyang Zhou, Xianyin Dai, Fang-Fang Shen, Ying-Ming Zhang,* Xiufang Xu, and Yu Liu*

Cite This: https://doi.org/10.1021/jacs.1c06741
Read Online
ACCESS | Metrics & More | Article Recommendations | Supporting Information

ABSTRACT: The construction of host–guest-binding-induced phosphorescent supramolecular assemblies has become one of increasingly significant topics in biomaterial research. Herein, we demonstrate that the cucurbit[8]uril host can induce the anthracene-conjugated bromophenylpyridinium guest to form a linear supramolecular assembly, thus facilitating the enhancement of red fluorescence emission by the host-stabilized charge-transfer interactions. When the anthryl group is photo-oxidized to anthraquinone, the obtained linear nanoconstructs can be readily converted into the homoternary inclusion complex, accompanied by the emergence of strong green phosphorescence in aqueous solution. More intriguingly, dual organelle-targeted imaging abilities have been also distinctively achieved in nuclei and lysosomes after undergoing photochemical reaction upon UV irradiation. This photooxidation-driven purely organic room-temperature phosphorescence provides a convenient and feasible strategy for supramolecular organelle identification to track specific biospecies and physiological events in the living cells.

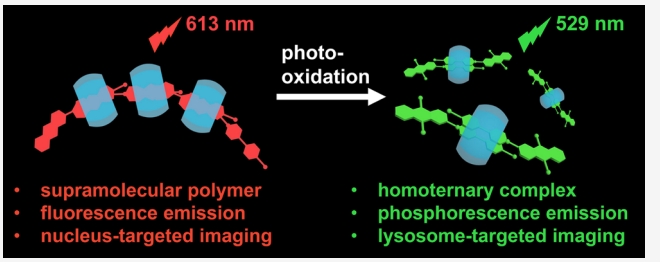

INTRODUCTION

Recently, considerable endeavors have been devoted to exploring light-emitting superstructures featuring persistent room-temperature phosphorescence (RTP), given their promising potentials in bioimaging,[1] optical switching,[2] and security protection.[3] Compared to the fluorescence-based nanosystems, the phosphorescence-based ones possess a longer lifetime, larger Stokes shift, and higher reliability working in complex biological environments.[4] Besides some conventional approaches (e.g., doping,[5] crystallization,[6] and polymerization[7]), host–guest complexation with cavity-bearing macrocycles, such as cyclodextrins[8] and cucurbiturils (CBs),[9] has emerged as an alternative and more powerful strategy to achieve purely organic RTP in both solution and the solid state, which has greatly expanded the research scope for supramolecular chemistry and biomaterial science.[10] Through the tight noncovalent encapsulation with optically active substrates, macrocyclic receptors can greatly promote the intersystem crossing (ISC) and simultaneously suppress the nonradiative relaxation processes, thus endowing supramolecular luminescent assemblies with high RTP efficiencies in a controllable manner.[11]

As for the fabrication of stimuli-responsive supramolecular nanoassemblies, a variety of stimuli-responsive units have been explored and utilized as building blocks that respond to chemical, biological, and physical factors.[12] Among these numerous external stimuli including pH change, coordination effect, enzymatic catalysis, and magnetic field, light input is believed as an ideal candidate, owing to its innate superiority of noninvasive and eco-friendly nature, as well as the fact that light irradiation as energy supply can trigger a series of configurational variations and photochemical reactions during a specified process, such as photoisomerism, photochromism, and photoinduced degradation and oxidation/reduction. In particular, anthracene-involved photochemical reactions, which combines the merits of remote-controllable characteristics of light input and rich reactivity of diverse chemical products, have been drawn into the limelight and viewed as a classic and reliable means of conferring desired photoresponsiveness to supramolecular assembled architectures.[13] In this context, many anthracene-derived building motifs, such as cyclodimers and endoperoxides, have been created to manipulate the molecular recognition properties of well-defined nanoconstructs.[14] Also, anthryl groups can be employed as elongated π-aromatic cores to control topological structures and fluorescence emission behaviors.[15] However, the rationally tunable photoluminescence using the anthracene-based fluorophores and phosphors has not been achieved in a single assembled entity, to the best of our knowledge. The

Received: June 29, 2021

development of highly efficient chemical stimuli approaches to regulate photoluminescent behaviors and related biological properties still remains an urgent challenge at the supramolecular level.[16]

For this purpose, it prompts us to consider an integration of CB-involved host−guest complexation and anthracene-involved photooxidation reaction as a coregulatory strategy for attaining advanced stimuli-responsive nanostructures with tunable fluorescence and RTP emission. In this work, the anthracene-conjugated bromophenylpyridinium salt (ANPY) was synthesized as a heteroditopic guest, which could form a stable inclusion complex with cucurbit[8]uril (CB[8]) via the host-stabilized intermolecular charge-transfer (CT) interactions. When the anthryl group of ANPY was photooxidized to anthraquinone under UV irradiation, the assembling modes were accordingly changed from "head-to-tail" supramolecular polymer to "head-to-head" homoternary inclusion complex. Moreover, ANPY and its photooxidation product AQPY displayed strikingly distinctive macrocycle-binding-enhanced photophysical behaviors in aqueous solution; that is, red fluorescence in the ANPY⊂CB[8] assembly could be readily converted to green phosphorescence in AQPY⊂CB[8] complex. Unexpectedly and more interestingly, the assembly induced photoluminescence enhancement in this supramolecular system could be further employed for dual organelle-targeted imaging of nuclei and lysosomes in the living cells. Therefore, the present work featuring photooxidation-triggered luminescent conversion and organelle-specific localization will allow us to understand the structure−activity relationship in this interesting, interdisciplinary, but less known area of biorelated supramolecular chemistry.

RESULTS AND DISCUSSION

The construction of fluorescent ANPY⊂CB[8] linear supramolecular assembly and phosphorescent AQPY⊂CB[8] homoternary inclusion complex is depicted in Scheme 1. The guest molecule ANPY was synthesized via Zincke reaction and the compound characterization is shown in the Supporting Information (Chart S1 and Figures S1−S6). Next, the host−guest molecular binding behaviors between CB[8] and ANPY were preliminarily investigated by means of UV−vis spectroscopy. As discerned from Figure 1a, free ANPY exhibited three main absorption peaks at 250, 320, and 350 nm, respectively. A new absorption band was observed in the long-wavelength region around 420−550 nm upon stepwise addition of CB[8], accompanied by the appearance of three isosbestic points and large bathochromic shift. In addition, the color of the ANPY solution instantly turned to brilliant yellow in the presence of 1.0 equiv of CB[8]. These phenomena jointly confirmed the host-stabilized intermolecular charge transfer interaction arising from the $\pi-\pi$ stacking between the electron-rich anthryl group as the donor and the electron-deficient pyridinium group as the acceptor in ANPY⊂CB[8] assembly.[17] In addition, after validating the 1:1 binding stoichiometry by Job plot, the association constant (K_a) in ANPY⊂CB[8] complexation was determined as 2.78×10^6 and 2.34×10^6 M^{-1} in water and phosphate buffer solution (PBS, 0.01 M, pH 7.4), respectively, by nonlinear least-squares method, which would ensure the high stability in both inanimate milieu and living cells, as described below (Figures S16 and S17, Supporting Information).

To shed more light on the assembling mode, the anthracene-derived quaternary ammonium salt (AN) and the bromophenyl-methyl-pyridinium salt with chloride as counterion (PY) were synthesized as reference compounds (Figures S10−S12, Supporting Information). ^{1}H NMR spectra revealed that both phenylpyridinium and anthryl protons shifted to higher field in the presence of CB[8], corresponding to the formation of heteroternary inclusion complexes (Figure S19, Supporting Information). Moreover, ^{1}H NMR titration experiments demonstrated that all of the aromatic proton signals of ANPY became drastically broadened and underwent pronounced upfield shifts with CB[8], indicative of the existence of large-sized nanoaggregates in solution (Figure S18,

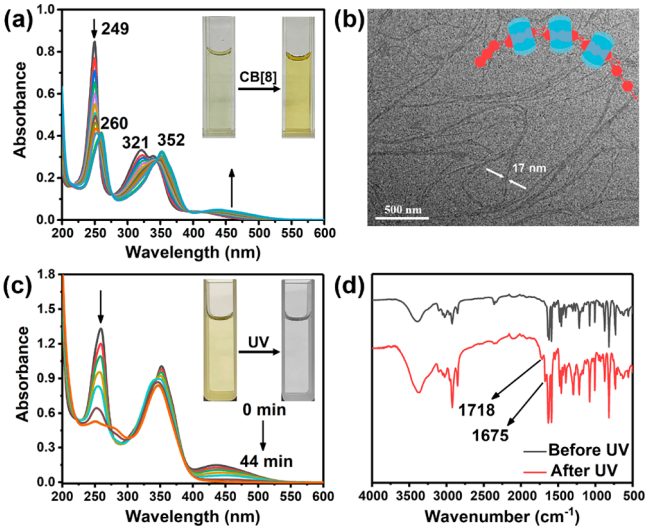

Figure 1. (a) UV−vis spectral changes of ANPY upon addition of CB[8] in H_2O at 298 K ([ANPY] = 1.0×10^{-5} M and [CB[8]] = 0−2.4×10^{-5} M). Inset: photographs of ANPY and ANPY⊂CB[8] solution. (b) TEM image of ANPY⊂CB[8] assembly. (c) UV−vis spectral changes of ANPY⊂CB[8] assembly versus different time of UV irradiation in H_2O at 298 K (λ = 365 nm, [ANPY] = [CB[8]] = 4.0×10^{-5} M). Inset: photographs of ANPY⊂CB[8] solution before and after UV light irradiation. (d) FTIR spectra of ANPY before and after UV irradiation.

Scheme 1. Schematic Illustration of Phototunable Conversion from Red Fluorescence to Green Phosphorescence Emission in the ANPY⊂CB[8] and AQPY⊂CB[8] Assemblies

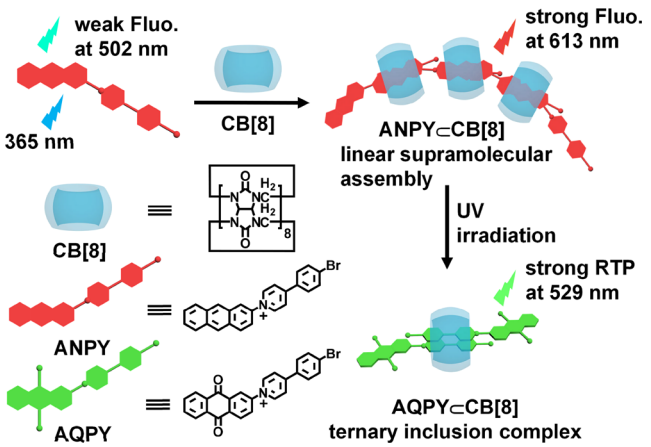

https://doi.org/10.1021/jacs.1c06741
J. Am. Chem. Soc. XXXX, XXX, XXX−XXX

Supporting Information). Meanwhile, as investigated by diffusion-ordered spectroscopy (DOSY), when the concentration of ANPY was fixed at 0.5 mM, the diffusion coefficients sharply decreased from 3.45×10^{-10} to 1.40×10^{-10} m^2/s before and after addition of CB[8], respectively, and the apparent degree of polymerization was calculated as approximately 15 on the basis of the Stokes−Einstein equation[18] (Figures S20 and S21, Supporting Information). Accordingly, the transmission electron microscopic image also showed that ANPY⊂CB[8] assembly mainly existed as fibrous nanoaggregates with width of 17 nm and lengths of several micrometers, which was contributed to a secondary aggregation of several linear ANPY⊂CB8 assemblies at high concentration in the dried state (Figure 1b). Also, the average hydrodynamic diameter was measured as 796 nm (Figure S22, Supporting Information). Taken together, these results substantiated that the inclusion complexation between CB[8] and ANPY could lead to the formation of linear supramolecular polymers in aqueous solution through multiple host-enhanced intermolecular CT interactions.

On account of photoactive anthracene that is prone to react with singlet oxygen ($^1O_2$) and generate anthraquinone as the complete photooxidation product,[19] we next monitored the photoreaction process of ANPY upon excitation by UV irradiation. No structural change was observed in ANPY under nitrogen atmosphere, whereas the NMR spectra became quite different after UV irradiation in air (Figure S23, Supporting Information). Meanwhile, UV absorption intensity of ANPY gradually decreased and the equilibrium state was achieved in 4 h (Figure S24, Supporting Information). These spectroscopic phenomena suggested that oxygen molecules got involved in the photochemical reaction with ANPY. It is also noteworthy that the photooxidation process could be significantly accelerated with assistance of CB[8] under the same experimental conditions. As can be seen from Figure 1c, along with the disappearance of CT band around 450 nm and color change of ANPY⊂CB[8] solution from yellow to colorless, the equilibrium state could be readily achieved in only 44 min in water. The evidence on the structural changes from anthracene to anthraquinone came from infrared (IR) absorption and mass spectrometry. Two new vibrational bands at 1675 and 1718 cm^{-1} emerged in the FTIR spectrum of ANPY after UV irradiation, which could be assigned to the characteristic stretching vibration of carbonyl group (Figure 1d). Meanwhile, the m/z peak at 440.0288 could be clearly assigned to AQPY, and no remaining ANPY was found in the presence of CB[8] (Figures S25 and S26, Supporting Information). Computational analyses further demonstrated that compared to pristine anthracene, the introduction of phenylpyridinium group and heavy bromine atom could greatly promote the spin−orbit coupling (SOC) of low-lying states in ANPY and boost the ISC from singlet to triplet excited states, thus facilitating the generation of $^1O_2$ and the production of anthraquinone-derived pyridinium salt AQPY (Figure S27, Supporting Information).[20] Indeed, the existence of $^1O_2$ species as a highly active intermediate has been trapped and characterized by its typical triple peaks in the electron paramagnetic resonance spectrum (Figure S28, Supporting Information).

To investigate the molecular binding mode of AQPY⊂CB[8] assembly, ^1H NMR titration experiments were performed by using PY and anthraquinone-derived quaternary ammonium salt (AQ) as the reference compounds (Figures S13−S15, Supporting Information). The proton signals of the mixtures of AQ, PY, and CB[8] resembled the simple superposition of free AQ and the PY⊂CB[8] complex, implying that CB[8] had a strong tendency to simultaneously accommodate two PY units rather than AQ in its cavity (Figure S29, Supporting Information). The m/z peaks at 1104.2 and 1106.1 in mass spectrum also revealed the formation of homoternary AQPY⊂CB[8] complex (Figure S30, Supporting Information). To thoroughly explore the photooxidation process, AQPY was directly synthesized via a similar method (Chart S1 and Figures S7−S9, Supporting Information). The structural characterization of synthesized product AQPY was in accordance with the one of photooxidized product, further corroborating the generation of anthraquinonyl derivative (Figures S31 and S32, Supporting Information). Different from the supramolecular polymers of ANPY⊂CB[8] assembly, the AQPY⊂CB[8] complex gave the irregular flake-like morphology in the TEM image, along with an average hydrodynamic diameter of ca. 228 nm (Figure S33, Supporting Information). These results probably contributed to the intermolecularly hydrophobic and $\pi-\pi$ interactions with the exposed anthraquinonyl group in AQPY. With the synthesized product AQPY in hand, it is found that the aromatic proton signals of AQPY underwent a dramatic complex-induced upfield shift upon addition of CB[8] and the chemical shift changes reached the equilibrium state with 0.5 equiv of CB[8] (Figure S34, Supporting Information). In addition, spectroscopic titration results demonstrated that the K_a values in the AQPY⊂CB[8] complexation were obtained as 3.13×10^{12} and 6.98×10^{11} M^{-2} in water and PBS, respectively, with a clear 1:2 binding stoichiometry (Figures S35, Supporting Information). Collectively, these results convincingly demonstrated that triggered by the photooxidation from anthracene to anthraquinone, the ANPY⊂CB[8] supramolecular polymers could be readily converted into the AQPY⊂CB[8] homoternary complex.

Subsequently, the optical properties have been characterized by photoluminescence spectroscopy in aqueous solution. As judged from Figure 2a, the individual ANPY showed fairly weak fluorescence emission at 502 nm. The emergence of new emission centered at 613 nm was observed upon addition of CB[8] into ANPY solution, mainly due to the formation of supramolecularly polymeric species with more extensive π-conjugated and rigidified structures. Interestingly, when irradiated with UV light at 365 nm, the emission peak at 613 nm gradually decreased with the appearance of a new peak at 521 nm, and the luminescent colors were changed from orange-red to green with continuous UV irradiation, as depicted by the CIE 1931 chromaticity diagram (Figure 2b,e,f). With a delay time of 0.2 ms, no emission at 613 nm was observed in the phosphorescence spectra and only the emission at 529 nm was maintained and enhanced with the prolonged UV irradiation time. The intensity of phosphorescence emission was 3.61 times as strong as that of fluorescence emission at 529 nm under the same conditions (Figures S36 and S37a, Supporting Information). Moreover, when N_2 was bubbled into the solution, the emission intensity at 529 nm further increased under oxygen-free condition (Figures S37b, Supporting Information). At the same time, time-resolved decay curves revealed that the lifetime measured at 613 nm was on the order of nanoseconds for ANPY⊂CB[8] assembly (1.15 ns), while the one measured at 529 nm was on the order of microseconds for AQPY⊂CB[8] complex (376.53

https://doi.org/10.1021/jacs.1c06741
J. Am. Chem. Soc. XXXX, XXX, XXX−XXX

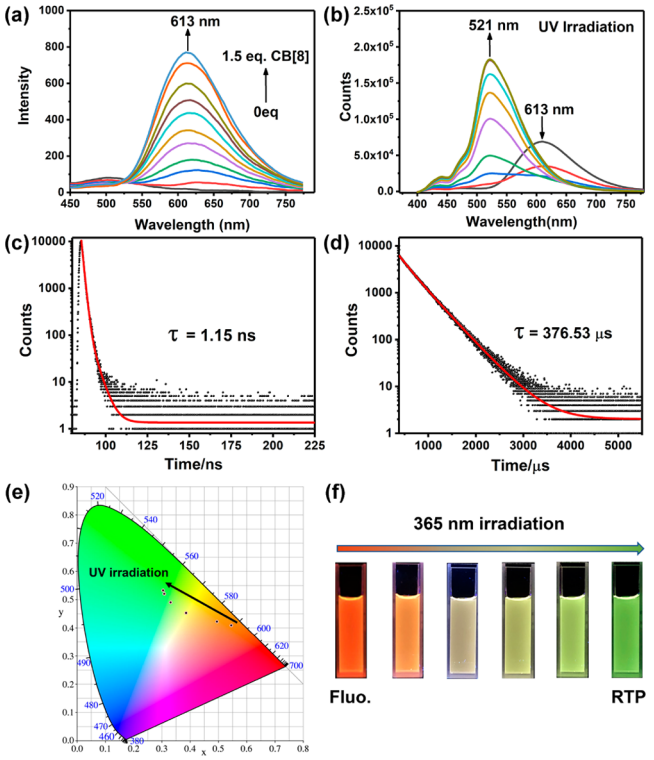

Figure 2. (a) Fluorescence spectra of ANPY upon addition of CB[8] in H_2O at 298 K ([ANPY] = 4.0 × 10^{-5} M and [CB[8]] = 0−6.0 × 10^{-5} M). (b) Prompt photoluminescence spectra and (c) fluorescence lifetime decay curves of ANPY⊂CB[8] assembly at 613 nm. (d) Phosphorescence lifetime decay curve of AQPY⊂CB[8] assembly at 529 nm. (e) The 1931 CIE chromaticity diagram illustrating the luminescent color changes and (f) luminescence photographs of ANPY⊂CB[8] assembly with continuous UV irradiation (λ_{ex} = 365 nm, 298 K).

μs, Figure 2c,d). Meanwhile, the emission intensity at 529 nm was significantly enhanced and the lifetime could reach up to 14.14 ms at the temperature of 77 K (Figure S38, Supporting Information). The quantum yields of ANPY and AQPY upon complexation with CB[8] were obtained as 2.06% and 1.53%, respectively (Figure S39, Supporting Information). By comparing these obtained photophysical data with the known CB-based nanosystems with RTP properties, we can reasonably infer that the photoluminescent emission at 613 and 529 nm is contributed to the short-lived fluorescent ANPY⊂CB[8] assembly and the long-lived phosphorescent AQPY⊂CB[8] complex, respectively.[21,22] In addition, similar to the spectroscopic results obtained in water, the photooxidation reaction process could be completed in PBS in 44 min and no obvious spectral difference was observed in water or PBS (Figures S40 and S41, Supporting Information). Also, there was no spectral change in the UV−vis absorbance spectra with or without fetal bovine serum (FBS), implying that these obtained supramolecular complexes could not be disassembled in the presence of FBS as competitive protein (Figure S42, Supporting Information). Apparently, the high stability of these supramolecular assemblies in different media would ensure the good biocompatibility and durability in biological fluids.

To deepen the understanding of the molecular binding modes, density functional theory (DFT) calculations were carried out by the Gaussian 16 program. From the perspective of energetics, the "head-to-tail" structure possessed minimum binding energy, which could be considered as the most stable molecular geometry among three possible inclusion modes of ANPY⊂CB[8] assembly (−47.7 kcal/mol in Figure S43 and Table S1, Supporting Information). Two optimized structures and their relative energies of supramolecular polymer fragments were also calculated. The results showed that the ANPY⊂CB[8] supramolecular polymers were more likely to grow as nonlinear chains in a ladder-shaped pattern, by which the undesirable steric hindrance can be avoided between two adjacent ANPY molecules (Figure S44 and Table S2, Supporting Information). Furthermore, as can be seen from the optimized molecular structures in Figure 3a,b, there are

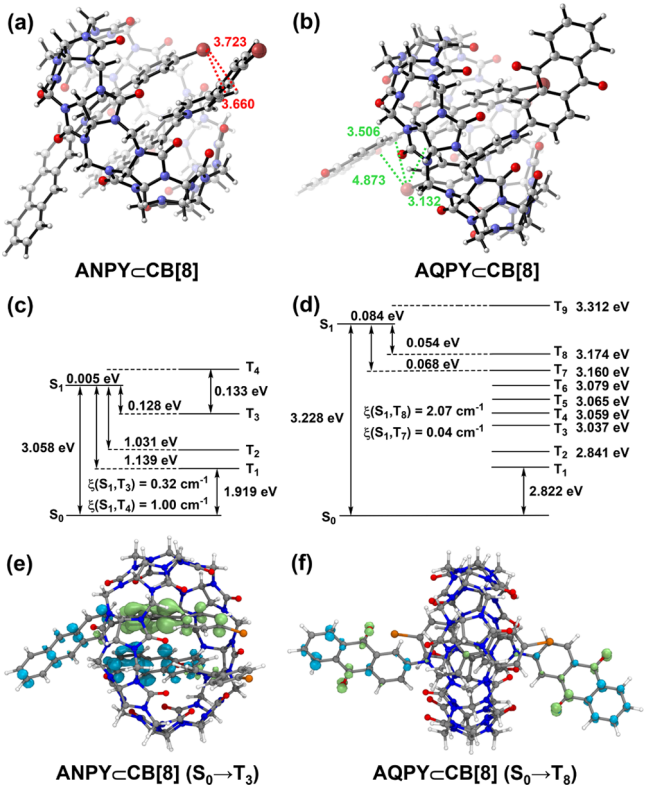

Figure 3. Optimized molecular geometries of (a) ANPY⊂CB[8] and (b) AQPY⊂CB[8] complexes; energy-level diagrams and SOC coefficients in (c) ANPY⊂CB[8] and (d) AQPY⊂CB[8] complexes; real space representation of hole and electron distributions of (e) ANPY⊂CB[8] and (f) AQPY⊂CB[8] complexes. Green and blue regions denote the electron and hole distributions, respectively.

extensive halogen-bonding connections in AQPY⊂CB[8] complex, such as C−Br···pyridine (3.506 Å) and C−Br···O (4.873 Å). Besides, the interatomic distance of C−Br···H−C in the AQPY⊂CB[8] complex (3.132 Å) is much shorter than the one in the ANPY⊂CB[8] complex (3.723 Å). Meanwhile, as shown in Figure 3c,d and Table S3, the transition energy from S_0 state to S_1 state is 3.228 eV in the AQPY⊂CB[8] complex, which is slightly larger than that in the ANPY⊂CB[8] complex (3.058 eV). However, the energy gap corresponding to the single−triplet excited states (ΔE_{ST}) for the AQPY⊂CB[8] complex ($S_1 \rightarrow T_8$, 0.054 eV) is smaller than that for the ANPY⊂CB[8] complex ($S_1 \rightarrow T_3$, 0.128 eV). In addition, the AQPY⊂CB[8] complex has a significantly larger SOC coefficient ($\xi(S_1, T_8)$, 2.07 cm^{-1}) than that of the ANPY⊂CB[8] complex ($\xi(S_1, T_3)$, 0.32 cm^{-1}). It is known

https://doi.org/10.1021/jacs.1c06741
J. Am. Chem. Soc. XXXX, XXX, XXX−XXX

that the intersystem crossing rate (k_{isc}) is mainly determined by both ΔE_{ST} and ξ_{ST} values.[23] Therefore, with much smaller ΔE_{ST} and larger ξ_{ST}, the k_{isc} of the AQPY⊂CB[8] complex could be significantly higher than the one of ANPY⊂CB[8] assembly, which was a prerequisite for efficient RTP. Collectively, benefiting from extensive halogen-bonding interactions and favorable radiative pathway, more efficient ISC and phosphorescence emission could be achieved in the AQPY⊂CB[8] supramolecular system.[24]

To gain more insights into the photophysical origins, hole−electron analyses were further performed on the obtained inclusion complexes. In the ANPY⊂CB[8] complex, the electron and hole distributions were initially located on the pyridyl and anthryl rings, respectively, indicating that the electrons were transferred from the electron-rich anthracene to the electron-deficient pyridine upon excitation (Figure S45a, Supporting Information). Then, the hole distribution on the anthryl ring decreased, which implied that part of the electrons flowing into the pyridyl ring returned to the anthryl ring via ISC from S_1 state to T_3 state (Figure 3e). Comparatively, in the AQPY⊂CB[8] complex, the lone pair of electrons on the carbonyl oxygen was excited to the adjacent phenyl ring at the S_1 state (Figure S45b, Supporting Information). As evidenced by the increased hole distribution and the decreased electron distribution, the electrons could be transferred from the phenyl ring to the adjacent carbonyl oxygen via ISC from S_1 state to T_8 state (Figure 3f).

Considering that biological imaging with precise positioning and responsiveness has great potential in biosensing and diagnosis, we were curious to know whether the conversion from fluorescence to phosphorescence could be utilized in the organelle-targeted cell imaging. Thus, confocal laser scanning microscopic experiments were carried out to explore the subcellular distribution of these obtained supramolecular assemblies. Human lung adenocarcinoma cells (A549 cell line) were treated with ANPY⊂CB[8] and then stained with Hoechst 33342, a commercial fluorescent dye for nuclei staining. As shown in Figure 4a−d, the red fluorescence emission assigned to ANPY⊂CB[8] assembly perfectly overlapped with the blue region of Hoechst 33342 (Pearson correlation coefficient, $\rho = 0.94$), implying that ANPY⊂CB[8] could preferentially accumulate in cell nuclei. Moreover, our results also suggest that due to the primary inclusion complexation with CB[8] and the secondary assembling process with DNA, the fluorescent sensing ability of ANPY could be greatly improved, which may be responsible for the nuclei-selective imaging in the living cells (Figure S46a,b, Supporting Information).[25] The apparent binding constants of ANPY and ANPY⊂CB[8] assembly with ctDNA were accordingly calculated as 2.67×10^4 and 2.81×10^4 M^{-1}, respectively, by means of fluorescence spectral titration experiments (Figure S46c,d, Supporting Information). Meanwhile, although both ANPY and ANPY⊂CB[8] assembly showed good nuclei-targeting abilities, the cytotoxicity of ANPY could be largely reduced with assistance of CB[8] (Figures S47 and S48, Supporting Information). In addition, bright red emission was exclusively observed in the nuclei after incubation in 30 min, exhibiting the time-dependent internalization and accumulation behaviors (Figure S49, Supporting Information).

Furthermore, the costaining of Lysotracker Blue and the AQPY⊂CB[8] complex gave good localization of blue fluorescence and green phosphorescence in lysosome,

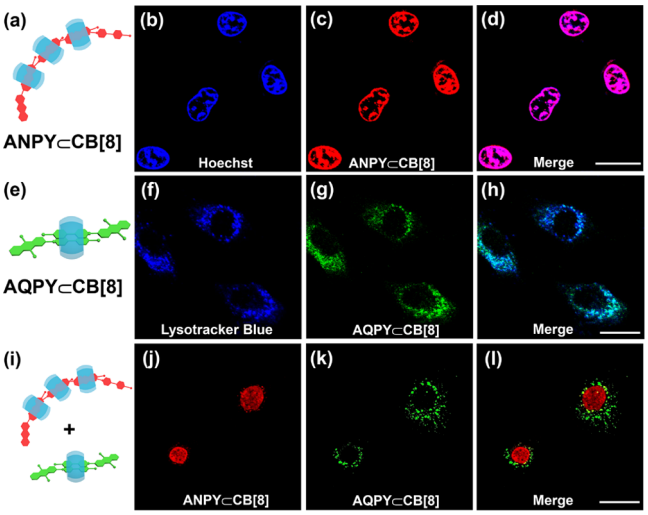

Figure 4. Confocal microscopic images of A549 cells costained with (a−d) Hoechst 33342 and ANPY⊂CB[8] assembly; (e−h) Lysotracker Blue and AQPY⊂CB[8] complex; (i−l) ANPY⊂CB[8] assembly after UV irradiation for 30 min. The excitation wavelengths were set as 405 nm ([ANPY] = [AQPY] = [CB[8]] = 8.0×10^{-6} M and scale bar = 30 μm).

indicative of the lysosome-targeting ability of the AQPY⊂CB[8] complex under cellular environment (Pearson correlation coefficient, $\rho = 0.90$, Figure 4e−h). Although both AQPY and AQPY⊂CB[8] assembly were almost noncytotoxic at the examined concentrations, only faint blue emission was observed when the cells were incubated with AQPY alone, implying that CB[8] plays an indispensable role in producing RTP (Figures S48, S50, and S51, Supporting Information). In addition, no spectral change in UV absorbance was observed in a wide pH range, indicative of the high stability of the AQPY⊂CB[8] complex in the low-pH lysosomal environment (Figure S52, Supporting Information). In our case, compared to the *n*:*n* ANPY⊂CB[8] assembly, the 2:1 AQPY⊂CB[8] complex with high charge density and strong electrostatic repulsive interactions probably changed the lipophilicity and decreased the electrophoretic force, which is beneficial for the lysosomal localization.[26] Remarkably, when the ANPY⊂CB[8] complex underwent insufficient photooxidation (i.e., UV irradiation for 30 min) in the extracellular milieu and then the corresponding solution was coincubated with the A549 cells, it is found that nuclei and lysosomes could be simultaneously visualized with high resolution (Figure 4i−l).

Finally, the photostability of the obtained supramolecular complexes were studied. There was no light fading in the distribution area of red fluorescence emission after laser irradiation for 15 min, indicating that the ANPY⊂CB[8] assembly was stable enough to be used as a positioning imaging agent for the nucleus (Figure S53, Supporting Information). In comparison, as for the AQPY⊂CB[8] complex, the green phosphorescence could be maintained for 10 min, whereas serious photobleaching was observed using the commercially available Lysotracker Blue in only 3 min under the same experimental conditions (Figure S54, Supporting Information). More interestingly, when the cells were costained with the ANPY⊂CB[8] assembly and Lysotracker Blue, red fluorescence was initially observed in nuclei and subsequently, strong phosphorescence appeared in the green channel in the range of 500−545 nm under

https://doi.org/10.1021/jacs.1c06741
J. Am. Chem. Soc. XXXX, XXX, XXX−XXX

continuous light irradiation for 2 min, which coincided with the blue region of Lysotracker Blue (Figure S55, Supporting Information). These phenomena indicate that the ANPY⊂CB[8] supramolecular polymer could be recombined as the AQPY⊂CB[8] ternary complex in cells when exposed to light irradiation, accompanied by the photophysical conversion from red fluorescence in nuclei to green phosphorescence in lysosomes. As we know, specific cell-staining systems are mostly achieved by the covalent attachment of different organelle-targeting agents onto chromophoric backbones.[27] It is necessary to develop novel labeling and positioning methods without tedious chemical synthesis or purification. These results provided us with an unusual photooxidation-based supramolecular regulation for multicolor targeted imaging of different organelles in the living cells.

CONCLUSION

In conclusion, a supramolecular luminescent nanosystem has been constructed via the host−guest complexation between CB[8] and ANPY, which is capable of phototunable conversion from fluorescence to phosphorescence in aqueous media and dual organelle-targeted imaging in different organelles. The CB-stabilized CT interactions can extend π-conjugation in ANPY⊂CB[8] supramolecular polymer, eventually resulting in the enhancement of red fluorescence emission at 613 nm. Meanwhile, the anthryl group in ANPY can be transformed into anthraquinonyl group in AQPY under UV irradiation, accompanied by the recombination of homoternary complex and the emergence of strong green phosphorescence at 529 nm. Remarkably, as investigated by the cell-staining experiments, these obtained nanostructures with unique assembly induced photoluminescent behaviors possess different positioning abilities in nuclei and lysosomes, which can be simply tuned by the duration of illumination. Thus, we can envision that the present results shown in this work can be of great value and will make significant contribution in creation of stimuli-responsive materials and in situ visualization of vital physiological events in cells.

ASSOCIATED CONTENT

Supporting Information

The Supporting Information is available free of charge at https://pubs.acs.org/doi/10.1021/jacs.1c06741.

Compound characterization, Job plot, K_a value, supramolecular polymer characterization, photooxidation product analysis and mechanism, molecular binding behaviors of homoternary complex, photoluminescence properties, theoretical calculation, cell viability, organelle specificity of complexes, and photostability data (PDF)

AUTHOR INFORMATION

Corresponding Authors

Yu Liu − *College of Chemistry, State Key Laboratory of Elemento-Organic Chemistry, Nankai University, Tianjin 300071, P. R. China;* orcid.org/0000-0001-8723-1896; Email: yuliu@nankai.edu.cn

Ying-Ming Zhang − *College of Chemistry, State Key Laboratory of Elemento-Organic Chemistry, Nankai University, Tianjin 300071, P. R. China*; Email: ymzhang@nankai.edu.cn

Authors

Hua-Jiang Yu − *College of Chemistry, State Key Laboratory of Elemento-Organic Chemistry, Nankai University, Tianjin 300071, P. R. China*

Qingyang Zhou − *College of Chemistry, State Key Laboratory of Elemento-Organic Chemistry, Nankai University, Tianjin 300071, P. R. China;* orcid.org/0000-0002-5267-8513

Xianyin Dai − *College of Chemistry, State Key Laboratory of Elemento-Organic Chemistry, Nankai University, Tianjin 300071, P. R. China*

Fang-Fang Shen − *College of Chemistry, State Key Laboratory of Elemento-Organic Chemistry, Nankai University, Tianjin 300071, P. R. China*

Xiufang Xu − *College of Chemistry, State Key Laboratory of Elemento-Organic Chemistry, Nankai University, Tianjin 300071, P. R. China;* orcid.org/0000-0002-3510-3267

Complete contact information is available at: https://pubs.acs.org/10.1021/jacs.1c06741

Notes

The authors declare no competing financial interest.

ACKNOWLEDGMENTS

This work was financially supported by the National Natural Science Foundation of China (Grants 21871154, 21772099, 21861132001, and 21873051) and the Fundamental Research Funds for the Central Universities, Nankai University. Dedicated to the 100th anniversary of Chemistry at Nankai University.

REFERENCES

(1) (a) Zhao, Q.; Huang, C.; Li, F. Phosphorescent Heavy-Metal Complexes for Bioimaging. *Chem. Soc. Rev.* **2011**, *40*, 2508−2524. (b) Shaikh, S.; Wang, Y.; ur Rehman, F.; Jiang, H.; Wang, X. Phosphorescent Ir(III) Complexes as Cellular Staining Agents for Biomedical Molecular Imaging. *Coord. Chem. Rev.* **2020**, *416*, 213344. (c) Wang, X.-F.; Xiao, H.; Chen, P.-Z.; Yang, Q.-Z.; Chen, B.; Tung, C.-H.; Chen, Y.-Z.; Wu, L.-Z. Pure Organic Room Temperature Phosphorescence from Excited Dimers in Self-Assembled Nanoparticles under Visible and Near-Infrared Irradiation in Water. *J. Am. Chem. Soc.* **2019**, *141*, 5045−5050. (d) Dang, Q.; Jiang, Y.; Wang, J.; Wang, J.; Zhang, Q.; Zhang, M.; Luo, S.; Xie, Y.; Pu, K.; Li, Q.; Li, Z. Room-Temperature Phosphorescence Resonance Energy Transfer for Construction of Near-Infrared Afterglow Imaging Agents. *Adv. Mater.* **2020**, *32*, 2006752.

(2) (a) Ma, X.; Wang, J.; Tian, H. Assembling-Induced Emission: An Efficient Approach for Amorphous Metal-Free Organic Emitting Materials with Room Temperature Phosphorescence. *Acc. Chem. Res.* **2019**, *52*, 738−748. (b) Gu, L.; Shi, H.; Gu, M.; Ling, K.; Ma, H.; Cai, S.; Song, L.; Ma, C.; Li, H.; Xing, G.; Hang, X.; Li, J.; Gao, Y.; Yao, W.; Shuai, Z.; An, Z.; Liu, X.; Huang, W. Dynamic Ultralong Organic Phosphorescence by Photoactivation. *Angew. Chem., Int. Ed.* **2018**, *57*, 8425−8431. (c) Liu, G.; Zhao, Y. Switching between Phosphorescence and Fluorescence Controlled by Chiral Self-Assembly. *Adv. Sci.* **2017**, *4*, 1700021.

(3) Li, Q.; Li, Z. Molecular Packing: Another Key Point for the Performance of Organic and Polymeric Optoelectronic Materials. *Acc. Chem. Res.* **2020**, *53*, 962−973. (b) Kwon, M. S.; Lee, D.; Seo, S.; Jung, J.; Kim, J. Tailoring Intermolecular Interactions for Efficient Room-Temperature Phosphorescence from Purely Organic Materials in Amorphous Polymer Matrices. *Angew. Chem., Int. Ed.* **2014**, *53*, 11177−11181. (c) Wan, S.; Lu, W. Reversible Photoactivated Phosphorescence of Gold(I) Arylethynyl Complexes in Aerated DMSO Solutions and Gels. *Angew. Chem., Int. Ed.* **2017**, *56*, 1784−1788. (d) Su, Y.; Zhang, Y.; Wang, Z.; Gao, W.; Jia, P.; Zhang, D.;

Yang, C.; Li, Y.; Zhao, Y. Excitation-Dependent Long-Life Luminescent Polymeric Systems under Ambient Conditions. *Angew. Chem., Int. Ed.* **2020**, *59*, 9967−9971.
(4) (a) Kuila, S.; Rao, K. V.; Garain, S.; Samanta, P. K.; Das, S.; Pati, S. K.; Eswaramoorthy, M.; George, S. J. Aqueous Phase Phosphorescence: Ambient Triplet Harvesting of Purely Organic Phosphors via Supramolecular Scaffolding. *Angew. Chem., Int. Ed.* **2018**, *57*, 17115−17119. (b) Zhang, G.; Palmer, G. M.; Dewhirst, M. W.; Fraser, C. L. A Dual-Emissive-Materials Design Concept Enables Tumour Hypoxia Imaging. *Nat. Mater.* **2009**, *8*, 747−751.
(5) (a) Lin, Z.; Kabe, R.; Nishimura, N.; Jinnai, K.; Adachi, C. Organic Long-Persistent Luminescence from a Flexible and Transparent Doped Polymer. *Adv. Mater.* **2018**, *30*, 1803713. (b) Lee, D.; Bolton, O.; Kim, B. C.; Youk, J. H.; Takayama, S.; Kim, J. Room Temperature Phosphorescence of Metal-Free Organic Materials in Amorphous Polymer Matrices. *J. Am. Chem. Soc.* **2013**, *135*, 6325−6329.
(6) (a) He, Z.; Gao, H.; Zhang, S.; Zheng, S.; Wang, Y.; Zhao, Z.; Ding, D.; Yang, B.; Zhang, Y.; Yuan, W. Z. Achieving Persistent, Efficient, and Robust Room-Temperature Phosphorescence from Pure Organics for Versatile Applications. *Adv. Mater.* **2019**, *31*, 1807222. (b) He, Z.; Zhao, W.; Lam, J. W. Y.; Peng, Q.; Ma, H.; Liang, G.; Shuai, Z.; Tang, B. Z. White Light Emission from a Single Organic Molecule with Dual Phosphorescence at Room Temperature. *Nat. Commun.* **2017**, *8*, 416. (c) Fateminia, S. M. A.; Mao, Z.; Xu, S.; Yang, Z.; Chi, Z.; Liu, B. Organic Nanocrystals with Bright Red Persistent Room-Temperature Phosphorescence for Biological Applications. *Angew. Chem., Int. Ed.* **2017**, *56*, 12160−12164.
(7) (a) Ogoshi, T.; Tsuchida, H.; Kakuta, T.; Yamagishi, T.-a.; Taema, A.; Ono, T.; Sugimoto, M.; Mizuno, M. Ultralong Room-Temperature Phosphorescence from Amorphous Polymer Poly(Styrene Sulfonic Acid) in Air in the Dry Solid State. *Adv. Funct. Mater.* **2018**, *28*, 1707369. (b) Parke, S. M.; Hupf, E.; Matharu, G. K.; de Aguiar, I.; Xu, L.; Yu, H.; Boone, M. P.; de Souza, G. L. C.; McDonald, R.; Ferguson, M. J.; He, G.; Brown, A.; Rivard, E. Aerobic Solid State Red Phosphorescence from Benzobismole Monomers and Patternable Self-Assembled Block Copolymers. *Angew. Chem., Int. Ed.* **2018**, *57*, 14841−14846.
(8) (a) Harada, A.; Takashima, Y.; Nakahata, M. Supramolecular Polymeric Materials via Cyclodextrin-Guest Interactions. *Acc. Chem. Res.* **2014**, *47*, 2128−2140. (b) Liu, Z.; Dai, X.; Sun, Y.; Liu, Y. Organic Supramolecular Aggregates Based on Water-Soluble Cyclodextrins and Calixarenes. *Aggregate* **2020**, *1*, 31−44.
(9) Barrow, S. J.; Kasera, S.; Rowland, M. J.; del Barrio, J.; Scherman, O. A. Cucurbituril-Based Molecular Recognition. *Chem. Rev.* **2015**, *115*, 12320−12406.
(10) (a) Yu, X.; Liang, W.; Huang, Q.; Wu, W.; Chruma, J. J.; Yang, C. Room-Temperature Phosphorescent γ-Cyclodextrin-Cucurbit[6]uril-Cowheeled [4]Rotaxanes for Specific Sensing of Tryptophan. *Chem. Commun.* **2019**, *55*, 3156−3159. (b) Chen, H.; Xu, L.; Ma, X.; Tian, H. Room Temperature Phosphorescence of 4-Bromo-1,8-naphthalic Anhydride Derivative-Based Polyacrylamide Copolymer with Photo-Stimulated Responsiveness. *Polym. Chem.* **2016**, *7*, 3989−3992. (c) Zhang, Z.-Y.; Chen, Y.; Liu, Y. Efficient Room-Temperature Phosphorescence of a Solid-State Supramolecule Enhanced by Cucurbit[6]uril. *Angew. Chem., Int. Ed.* **2019**, *58*, 6028−6032. (d) Zhou, W.-L.; Chen, Y.; Yu, Q.; Zhang, H.; Liu, Z.-X.; Dai, X.-Y.; Li, J.-J.; Liu, Y. Ultralong Purely Organic Aqueous Phosphorescence Supramolecular Polymer for Targeted Tumor Cell Imaging. *Nat. Commun.* **2020**, *11*, 4655.
(11) Zhang, T.; Ma, X.; Wu, H.; Zhu, L.; Zhao, Y.; Tian, H. Molecular Engineering for Metal-Free Amorphous Materials with Room-Temperature Phosphorescence. *Angew. Chem., Int. Ed.* **2020**, *59*, 11206−11216.
(12) (a) Su, X.; Aprahamian, I. Hydrazone-Based Switches, Metallo-Assemblies and Sensors. *Chem. Soc. Rev.* **2014**, *43*, 1963−1981. (b) Kakuta, T.; Yamagishi, T.-a.; Ogoshi, T. Stimuli-Responsive Supramolecular Assemblies Constructed from Pillar[n]arenes. *Acc. Chem. Res.* **2018**, *51*, 1656−1666. (c) Xia, D.; Wang, P.; Ji, X.; Khashab, N. M.; Sessler, J. L.; Huang, F. Functional Supramolecular Polymeric Networks: The Marriage of Covalent Polymers and Macrocycle-Based Host−Guest Interactions. *Chem. Rev.* **2020**, *120*, 6070−6123. (d) Zhang, Y.-M.; Liu, Y.-H.; Liu, Y. Cyclodextrin-Based Multistimuli-Responsive Supramolecular Assemblies and Their Biological Functions. *Adv. Mater.* **2020**, *32*, 1806158. (e) Zhou, Z.; Vázquez-González, M.; Willner, I. Stimuli-Responsive Metal-Organic Framework Nanoparticles for Controlled Drug Delivery and Medical Applications. *Chem. Soc. Rev.* **2021**, *50*, 4541−4563.
(13) (a) FOX, M. A.; OLIVE, S. Photooxidation of Anthracene on Atmospheric Particulate Matter. *Science* **1979**, *205*, 582−583. (b) Gao, Z.; Han, Y.; Wang, F. Cooperative Supramolecular Polymers with Anthracene-Endoperoxide Photo-Switching for Fluorescent Anti-Counterfeiting. *Nat. Commun.* **2018**, *9*, 3977. (c) Zhou, Y.; Zhang, H.-Y.; Zhang, Z.-Y.; Liu, Y. Tunable Luminescent Lanthanide Supramolecular Assembly Based on Photoreaction of Anthracene. *J. Am. Chem. Soc.* **2017**, *139*, 7168−7171. (d) Wang, Y.-X.; Zhang, Y.-M.; Liu, Y. Photolysis of an Amphiphilic Assembly by Calixarene-Induced Aggregation. *J. Am. Chem. Soc.* **2015**, *137*, 4543−4549. (e) Li, T.; Ma, X. Host-Guest Supramolecular Amphiphile Enhanced Photodecomposition with Responsive Room-Temperature Phosphorescence Signals. *Dyes Pigm.* **2018**, *148*, 306−312.
(14) (a) Huang, Z.-A.; Chen, C.; Yang, X.-D.; Fan, X.-B.; Zhou, W.; Tung, C.-H.; Wu, L.-Z.; Cong, H. Synthesis of Oligoparaphenylene-Derived Nanohoops Employing an Anthracene Photodimerization−Cycloreversion Strategy. *J. Am. Chem. Soc.* **2016**, *138*, 11144−11147. (b) Omoto, K.; Tashiro, S.; Shionoya, M. Phase-Dependent Reactivity and Host−Guest Behaviors of a Metallo-Macrocycle in Liquid and Solid-State Photosensitized Oxygenation Reactions. *J. Am. Chem. Soc.* **2021**, *143*, 5406−5412.
(15) (a) Wu, G.; Szabó, I.; Rosta, E.; Scherman, O. A. Cucurbit[8]uril-Mediated Pseudo[2,3]rotaxanes. *Chem. Commun.* **2019**, *55*, 13227−13230. (b) Wu, G.; Bae, Y. J.; Olesińska, M.; Antón-García, D.; Szabó, I.; Rosta, E.; Wasielewski, M. R.; Scherman, O. A. Controlling the Structure and Photophysics of Fluorophore Dimers Using Multiple Cucurbit[8]uril Clampings. *Chem. Sci.* **2020**, *11*, 812−825.
(16) Zhang, Y.-M.; Zhang, N.-Y.; Xiao, K.; Yu, Q.; Liu, Y. Photo-Controlled Reversible Microtubule Assembly Mediated by Paclitaxel-Modified Cyclodextrin. *Angew. Chem., Int. Ed.* **2018**, *57*, 8649−8653. (b) Gong, L.; He, K.; Liu, J. Concentration-Dependent Subcellular Distribution of Ultrasmall Near-Infrared-Emitting Gold Nanoparticles. *Angew. Chem., Int. Ed.* **2021**, *60*, 5739−5743.
(17) (a) Liu, Y.; Yu, Y.; Gao, J.; Wang, Z.; Zhang, X. Water-Soluble Supramolecular Polymerization Driven by Multiple Host-Stabilized Charge-Transfer Interactions. *Angew. Chem., Int. Ed.* **2010**, *49*, 6576−6579. (b) Ko, Y. H.; Kim, K.; Kang, J.-K.; Chun, H.; Lee, J. W.; Sakamoto, S.; Yamaguchi, K.; Fettinger, J. C.; Kim, K. Designed Self-Assembly of Molecular Necklaces Using Host-Stabilized Charge-Transfer Interactions. *J. Am. Chem. Soc.* **2004**, *126*, 1932−1933. (c) Ji, Z.; Li, J.; Chen, G.; Jiang, M. Fate of Host-Stabilized Charge Transfer Complexation Based on Cucurbit[8]uril: Inducing Cyclization of PNIPAM and Dissociation in Self-Assembly of the Cyclic Polymer. *ACS Macro Lett.* **2016**, *5*, 588−592. (d) Assaf, K. I.; Alnajjar, M. A.; Nau, W. M. Supramolecular Assemblies through Host−Guest Complexation between Cucurbiturils and an Amphiphilic Guest Molecule. *Chem. Commun.* **2018**, *54*, 1734−1737.
(18) Kang, Y.; Cai, Z.; Huang, Z.; Tang, X.; Xu, J.-F.; Zhang, X. Controllable Supramolecular Polymerization Promoted by Host-Enhanced Photodimerization. *ACS Macro Lett.* **2016**, *5*, 1397−1401.
(19) (a) Alonso, R.; Jiménez, M. C.; Miranda, M. A. Stereodifferentiation in the Compartmentalized Photooxidation of a Protein-Bound Anthracene. *Org. Lett.* **2011**, *13*, 3860−3863. (b) Niu, E.-P.; Mau, A. W.-H.; Ghiggino, K. P. Dye-Sensitized Photooxidation of Anthracene and its Derivatives in Nafion Membrane. *Aust. J. Chem.* **1991**, *44*, 695−704. (c) Sugiyama, N.; Iwata, M.; Yoshioka, M.; Yamada, K.; Aoyama, H. Photooxidation of Anthracene. *Bull. Chem. Soc. Jpn.* **1969**, *42*, 1377−1379. (d) Yamashita, K.-i.; Sugiura, K.-i. Photochemical Reaction of Anthracene with

https://doi.org/10.1021/jacs.1c06741
J. Am. Chem. Soc. XXXX, XXX, XXX−XXX

Dioxygen Catalyzed by Platinum(II) Porphyrin. *Tetrahedron Lett.* **2019**, *60*, 151081.
(20) Toshima, N.; Sugano, T.; Hirai, H. The Effect of Heavy-Atom Solvents on the Photooxidation of Anthracene. *Can. J. Chem.* **1984**, *62*, 2047.
(21) Shen, F.-F.; Chen, Y.; Dai, X.; Zhang, H.-Y.; Zhang, B.; Liu, Y.; Liu, Y. Purely Organic Light-Harvesting Phosphorescence Energy Transfer by β-Cyclodextrin Pseudorotaxane for Mitochondria Targeted Imaging. *Chem. Sci.* **2021**, *12*, 1851−1857.
(22) Baryshnikov, G.; Minaev, B.; Ågren, H. Theory and Calculation of the Phosphorescence Phenomenon. *Chem. Rev.* **2017**, *117*, 6500−6537.
(23) Ma, H.; Peng, Q.; An, Z.; Huang, W.; Shuai, Z. Efficient and Long-Lived Room-Temperature Organic Phosphorescence: Theoretical Descriptors for Molecular Designs. *J. Am. Chem. Soc.* **2019**, *141*, 1010−1015.
(24) Peng, Q.; Ma, H.; Shuai, Z. Theory of Long-Lived Room-Temperature Phosphorescence in Organic Aggregates. *Acc. Chem. Res.* **2021**, *54*, 940−949.
(25) (a) Evenou, P.; Rossignol, J.; Pembouong, G.; Gothland, A.; Colesnic, D.; Barbeyron, R.; Rudiuk, S.; Marcelin, A.-G.; Ménand, M.; Baigl, D.; Calvez, V.; Bouteiller, L.; Sollogoub, M. Bridging β-Cyclodextrin Prevents Self-Inclusion, Promotes Supramolecular Polymerization, and Promotes Cooperative Interaction with Nucleic Acids. *Angew. Chem., Int. Ed.* **2018**, *57*, 7753−7758. (b) Fudickar, W.; Linker, T. Structural Motives Controlling the Binding Affinity of 9,10-Bis(methylpyridinium)anthracenes towards DNA. *Bioorg. Med. Chem.* **2020**, *28*, 115432.
(26) Wang, Y.; Yao, H.; Zhuang, Z.; Yao, J.; Zhou, J.; Zhao, Z. Photostable and Biocompatible AIE-Active Conjugated Polyelectrolytes for Efficient Heparin Detection and Specific Lysosome Labelling. *J. Mater. Chem. B* **2018**, *6*, 6360−6364.
(27) (a) Xu, W.; Lee, M. M. S.; Nie, J.-J.; Zhang, Z.; Kwok, R. T. K.; Lam, J. W. Y.; Xu, F.-J.; Wang, D.; Tang, B. Z. Three-Pronged Attack by Homologous Far-red/NIR AIEgens to Achieve 1 + 1 + 1 > 3 Synergistic Enhanced Photodynamic Therapy. *Angew. Chem., Int. Ed.* **2020**, *59*, 9610−9616. (b) Alamudi, S. H.; Satapathy, R.; Kim, J.; Su, D.; Ren, H.; Das, R.; Hu, L.; Alvarado-Martínez, E.; Lee, J. Y.; Hoppmann, C.; Peña-Cabrera, E.; Ha, H.-H.; Park, H.-S.; Wang, L.; Chang, Y.-T. Development of Background-Free Tame Fluorescent Probes for Intracellular Live Cell Imaging. *Nat. Commun.* **2016**, *7*, 11964.

https://doi.org/10.1021/jacs.1c06741
J. Am. Chem. Soc. XXXX, XXX, XXX−XXX